

## REVISION 2

# Crystallization experiments in rhyolitic systems: the effect of temperature cycling and starting material on crystal size distribution

Marize Muniz da Silva<sup>1,2\*</sup>, Francois Holtz<sup>1</sup> and Olivier Namur<sup>1</sup>

<sup>1</sup> Leibniz Universität Hannover, Institut of Mineralogy, Callinstr. 3, 30167, Hannover, Germany;

<sup>2</sup> Departamento de Geologia, Instituto de Geociências, Universidade Federal do Rio de Janeiro, Cidade Universitária, 21949-900 Ilha do Fundão, Rio de Janeiro, RJ, Brazil;

E-mail: [muniz.marize@gmail.com](mailto:muniz.marize@gmail.com); [f.holtz@mineralogie.uni-hannover.de](mailto:f.holtz@mineralogie.uni-hannover.de);

[o.namur@mineralogie.uni-hannover.de](mailto:o.namur@mineralogie.uni-hannover.de)

### Abstract

One of the various problems faced in experimental petrology is the fact that most experimental products obtained by crystallization experiments are too small, making their accurate identification by electron microprobe and laser ablation analyses very difficult. This problem is magnified when a highly polymerized starting material is used for experiments at low temperature (e.g. 700°C - 800°C). In this study, we present the results of crystallization experiments performed using a rhyolitic starting glass in which we test the potential of temperature cycling and pre-hydrated starting material to increase crystal size and discuss the effect of those variables on the attainment of chemical equilibrium. Experiments were performed at different temperatures (725 to 815°C) and pressures (1 and 2 kbar), under water-saturated conditions ( $a_{\text{H}_2\text{O}} = 1$ ; with  $a_{\text{H}_2\text{O}}$  being the water activity). During the experiments, temperature was either constant or cycled to  $\pm 15^\circ\text{C}$  around the target temperature during the first half of the runs. We used either a pre-hydrated (7 wt.%  $\text{H}_2\text{O}$ ) rhyolitic glass or a dry rhyolitic glass to which 7 wt.%  $\text{H}_2\text{O}$  was added during capsule preparation.

26 Our results differ between 1 and 2 kbar experiments. At 1 kbar, plagioclase and  
27 orthopyroxene were the main crystalline phases affected and temperature cycling ( $\pm 15^\circ\text{C}$ ) did  
28 not increase the crystal size of these phases. In contrast, if only the nature of the starting  
29 material is considered (dry glass vs. pre-hydrated), the use of a pre-hydrated starting material  
30 successfully increased the overall crystal size and decreased the crystal number density. At 2  
31 kbar, plagioclase and amphibole were the main phases and the largest crystals were also  
32 obtained when pre-hydrated starting material was used. Contrary to experiments at 1 kbar,  
33 temperature cycling also increased the overall crystal size. The different effects of  
34 temperature cycling at 1 and 2 kbar are attributed (1) to the different cation diffusivities at 1  
35 and 2 kbar caused by different melt water concentrations and (2) the negligible effect of  
36 temperature cycling at 1 kbar ( $\pm 15^\circ\text{C}$ ) is explained by little dissolution of phases, so that  
37 small crystals were already too large to be completely consumed by the dissolution process in  
38 the high temperature interval. The results demonstrate that temperature oscillation (depending  
39 on the amplitude) and the nature of the starting material (pre-hydrated vs. dry glass + water)  
40 are two parameters that can contribute to increase crystal sizes in experiments with rhyolitic  
41 melts. However, we also observed that the use of a pre-hydrated starting material increased  
42 the occurrence of zoned plagioclase crystals which may indicate that chemical equilibrium  
43 was not perfectly reached.

44 **Keywords:** Crystallization experiment, Temperature cycling, Crystal size distribution,  
45 Rhyolite

## 46 **Introduction**

47 Experimental petrology and high pressure technologies have been widely used in the last  
48 century to understand the crystallization history of magmatic systems. In addition, all  
49 thermodynamic models predicting liquid lines of descent are based on experimental  
50 databases. The pre-requisite for accurate models is that equilibrium between solid phases,  
51 fluids and silicate melts is reached. However, attaining complete equilibrium between highly

52 polymerized melts and silica-rich crystals, such as feldspar, is difficult and becomes even  
53 more complicated when crystallization experiments are performed under low temperature  
54 conditions (700 – 800°C). This is mainly due to the high viscosity of the melt that makes  
55 diffusion of chemical components very slow and extremely long experimental durations are  
56 thus needed to obtain complete chemical equilibration between crystals and melt (e.g.  
57 Pichavant et al. 2007; Fenn 1977).

58 Two fundamentally different methods to experimentally constrain phase equilibria in  
59 magmatic systems are generally used: crystallization experiments (e.g. Scaillet et al. 2016)  
60 and melting experiments (e.g., Rushmer 1995; Patino Douce et al. 1996; Patino Douce and  
61 Harris 1998). Phase equilibria experiments in dacitic to rhyolitic systems need to be  
62 conducted at low temperature (700°C – 900°C). At these conditions melting experiments  
63 usually fail to reach bulk equilibrium due to slow diffusion of chemical components. For  
64 melting experiments, if a natural rock powder with grain sizes of 30 – 60 µm is used as  
65 starting material, there will be a large proportion of minerals that may not reach complete  
66 equilibrium. This is commonly observed when using plutonic rock powders as starting  
67 material as well as volcanic rock powders, which contain microlites or phenocrysts (e.g,  
68 Venezky and Rutherford 1999; Shea and Hammer 2013). For crystallization experiments,  
69 synthetic oxide powders are often used (e.g. Charlier and Grove 2012; Nandedkar et al. 2014)  
70 and succeed in reaching equilibrium in high temperature experiments with basaltic systems.  
71 They can however lead to the formation of meta-stable phases in experiments with high  
72 viscosity melts (e.g. formation of mullite from Al<sub>2</sub>O<sub>3</sub>, for example; Holtz et al., 1992). The  
73 use of an amorphous phase such as a gel (e.g., Tuttle and Bowen 1958; James and Hamilton  
74 1969) or a glass (e.g., Pichavant 1987; Scaillet et al. 2016) is therefore better suited for phase  
75 equilibria experiments in silicic systems. With an amorphous starting material, equilibrium  
76 conditions are easier to reach in rhyolitic and dacitic systems, but experimental products  
77 usually contain extremely small crystals. These small crystals represent a severe limitation in

78 experimental petrology because they very often cannot be identified or accurately measured  
79 by methods such as electron microprobe or laser ablation inductively coupled plasma mass  
80 spectrometry (LA-ICPMS).

81 Temperature cycling during experiments has recently been proven extremely helpful  
82 to increase the size of crystals in basaltic systems at 1 atm (Mills & Glazner 2013) or under  
83 pressure (Erdmann & Koepke 2016), but the benefit of this approach has never been  
84 quantitatively tested in rhyolitic systems. Crystal nucleation and growth strongly depend on  
85 the degree of undercooling with low undercooling resulting in larger crystals (Lofgren, 1974;  
86 Fenn 1977). Thermal cycling provides another opportunity to form large crystals because  
87 components can be redistributed among phases. Melting the small crystals during heating  
88 episodes of a temperature oscillation may lead to the formation of larger crystals during the  
89 cooling episodes. Here we tested the potential of temperature cycling to increase crystal and  
90 melt pool sizes in a highly polymerized rhyolitic system at low temperature (725°C - 815°C)  
91 and moderate pressure (1 and 2 kbar). We also investigated the effect of temperature cycling  
92 on the attainment of chemical equilibrium. We used two different approaches to perform our  
93 crystallization experiments. The first approach, which is the most commonly applied in  
94 experimental petrology, is to use a dry glass powder to which we add water (or other  
95 volatiles) during capsule preparation. The second approach, which is less commonly used, is  
96 to pre-saturate the glass with volatiles using high pressure vessels. In the first case, the  
97 hydrous glass is produced during the experimental run by diffusion of H<sub>2</sub>O from a vapor  
98 phase into an initially dry glass. This implies that when the experiment starts, the fluid phase  
99 is heterogeneously distributed in the capsule. In the second approach, crystals grow from a  
100 melt in which volatiles are already distributed homogeneously. Our experiments show that  
101 temperature cycling does not affect phase relationships or composition of the crystals but may  
102 significantly increase crystal sizes, as does the use of pre-hydrated starting material.

103

## Methodology

## 104 **General experimental strategy**

105 The general methodology and the experimental conditions applied in this study are shown  
106 schematically in **Fig. 1** and are designed to compare four types of experimental approaches:  
107 crystallization from a dry powder plus added water during capsule preparation, with and  
108 without temperature cycling and crystallization from a pre-hydrated glass powder, with and  
109 without temperature cycling. We performed a total of 14 crystallization experiments on a  
110 single composition, at temperatures between 700°C and 815°C and pressures of 1 and 2 kbar.

111

## 112 **Starting material**

113 **Dry glasses:** All experiments were performed using a synthetic glass of rhyolitic composition  
114 prepared from a mixture of pure oxide (SiO<sub>2</sub>, TiO<sub>2</sub>, Al<sub>2</sub>O<sub>3</sub>, Fe<sub>2</sub>O<sub>3</sub>, MnO) and carbonate  
115 (CaCO<sub>3</sub>, Na<sub>2</sub>CO<sub>3</sub>, K<sub>2</sub>CO<sub>3</sub>) powders, mixed using an agate ball mill. The starting material was  
116 melted twice in a platinum crucible at a temperature of 1600°C and 1 atm for 4 hours,  
117 followed by immersion of the crucible in water for rapid quench. Between the two melting  
118 procedures, the sample was crushed and ground in a rotary mortar. The composition and  
119 homogeneity of the glass were determined by electron microprobe analyses (**Table 1**).

120

121 **Pre-hydrated glasses:** A total of three capsules were prepared where 93 wt.% of dry glass  
122 (400, 400 and 700 mg) and 7% wt.% of H<sub>2</sub>O were loaded in gold/palladium (Au<sub>80</sub>Pd<sub>20</sub>)  
123 capsules (to avoid Fe loss). Capsules were then run in an internally heated pressure vessel  
124 (IHPV) at 1200°C and at a pressure of 3 kbar for 24 hours. After the runs, the water content in  
125 the quenched glass was measured by Karl-Fischer titration (see details in Behrens et al. 1996).  
126 Measurements were performed on 10 to 24 mg of pre-hydrated material, which is sufficient to  
127 obtain reliable results with an uncertainty smaller than 0.15 wt.% H<sub>2</sub>O. To check the  
128 homogeneity of the samples, the analyzed aliquots were taken from the top and the bottom of

129 each gold/palladium capsule. Measured water concentrations range from 6.86 to 7.02 wt.%  
130 H<sub>2</sub>O and we did not find any obvious vertical variability.

131

132 **Capsule preparation for crystallization experiments:** (1) pre-hydrated starting material was  
133 crushed in a mortar and ~30 mg of this material were loaded in 12 mm long Au capsules (3.2  
134 mm outer diameter and 0.2 mm wall thickness) that were welded shut or (2) dry glass powder  
135 (93 wt.%; 30 mg) and 7 wt.% of deionized H<sub>2</sub>O were loaded into Au capsules (same size as  
136 before) and welded shut. To ensure that no fluid escaped during welding, the weight of the  
137 loaded capsule was measured before and after the welding procedure.

138

### 139 **Experimental Apparatus**

140 Crystallization experiments were performed at the Leibniz Universität Hannover (LUH) in  
141 Renee-41 cold-seal pressure vessels (CSPV). The CSPVs are arranged horizontally and water  
142 is used as the pressure medium. The temperature during the experiments was continuously  
143 recorded by an external sheathed K-type thermocouple, placed in a borehole at the end of the  
144 autoclave near the hot zone. The CSPVs are equipped with a ramp/soak temperature  
145 controller REX-P24 that allows automatic temperature oscillation as a function of time. The  
146 relation between the measured temperature (external thermocouple) and the temperature at the  
147 sample position was calibrated at: (1) atmospheric pressure in the temperature interval of 200  
148 to 850°C using a self-made calibration device and a certified thermocouple and (2) at 1 kbar  
149 over the same temperature interval using the self-made calibration device. This device  
150 consists of three K-type thermocouples positioned side by side, with three different lengths  
151 (positions A, B and C) covering the hot zone of the CSPV. Positions A, B and C are at 7, 27  
152 and 46 mm respectively from the end of the borehole of the vessel. The uncertainties of the  
153 thermocouples is  $\pm 1.3^\circ\text{C}$  for temperatures  $> 700^\circ\text{C}$  and  $\pm 0.6^\circ\text{C}$  for temperatures  $< 700^\circ\text{C}$ .  
154 During calibration, temperature fluctuations (in each position) were not higher than  $\pm 2^\circ\text{C}$  and

155 we estimated that the uncertainty of the temperature measured during experiments is  $\pm 5^{\circ}\text{C}$ .  
156 We found that the temperature gradient along the hot zone of the CSPV is variable and may  
157 reach up to  $60^{\circ}\text{C}$ . To minimize temperature variation during experiments, our capsules did not  
158 exceed 12 mm in length in order to fit in the position closest to the external thermocouple  
159 (position A). Water pressure was monitored with a transducer calibrated against a strain gauge  
160 monometer, with an uncertainty of  $\pm 0.03$  kbar. The amount of water needed to increase the  
161 pressure from 0 to 2 kbar is 300 ml. The intrinsic oxygen fugacity of the CSPV is close to  
162 NNO (Ni-NiO) oxygen fugacity buffer (Gardner et al. 1995).

163

#### 164 **Experimental procedure**

165 In each experimental run, two capsules were inserted into each CSPV and placed side by side  
166 in position A. For each run, one capsule contained a dry glass with 7 wt.%  $\text{H}_2\text{O}$  while the  
167 other one contained the pre-hydrated glass. The pressure vessel was then inserted into a pre-  
168 heated furnace and 20 to 30 minutes were sufficient to reach the target temperature. Run  
169 durations were 21 days for twelve experiments and 14 days for two experiments (Table 2). As  
170 shown in Fig. 1, we applied temperature cycling to some experiments. For cycled  
171 experiments, the temperature path was as follows: temperature oscillation was started at the  
172 beginning of the experiment, with a amplitude of  $+15^{\circ}\text{C}$  above and then  $-15^{\circ}\text{C}$  below the  
173 final equilibrium temperature (e.g.,  $725^{\circ}\text{C}$ ,  $750^{\circ}\text{C}$ ,  $775^{\circ}\text{C}$  and  $815^{\circ}\text{C}$ ). The variation of  $30^{\circ}\text{C}$   
174 between the high and low temperatures was attained within two hours ( $0.5^{\circ}\text{C}/\text{min}$ ). The upper  
175 and lower temperatures were held constant for one hour (Supplementary Dataset A). No  
176 significant pressure change ( $< 0.07$  kbar) was observed as a result of the temperature  
177 variation. Temperature cycling was conducted for 14 days (only 7 days for one of the  
178 experiments) and the temperature was then kept constant for another 7 days. At the end of the  
179 experiments, the products were quenched by cooling the autoclave with a stream of

180 compressed air for 30 to 40 minutes. During quenching, the pressure was kept constant until  
181 the autoclave reached  $\sim 20^{\circ}\text{C}$ . Pressure was then released.

182

### 183 **Analytical techniques**

184 Run products were mounted in epoxy and polished for analysis. Experiments were analyzed  
185 with an electron microprobe (Cameca SX100) at LUH. For mineral analysis, we used a  
186 focused beam with a current of 15 nA. For glasses, we used a beam current of 4 nA and a spot  
187 size of 10  $\mu\text{m}$ . Minerals and glasses were analyzed with an acceleration voltage of 15 kV.  
188 Counting times were 10 s on peaks and 5 s for background on both sides. Calibration of the  
189 electron microprobe was based on natural and synthetic standards: albite for Na; wollastonite  
190 for Ca and Si; orthoclase for K, Durango apatite for P;  $\text{Al}_2\text{O}_3$  for Al;  $\text{Mn}_2\text{O}_3$  for Mn;  $\text{TiO}_2$  for  
191 Ti; MgO for Mg; and  $\text{Fe}_2\text{O}_3$  for Fe. Calibrations were independently checked against external  
192 natural mineral standards: plagioclase (Labradorite) Lake County (USNM 115900);  
193 hornblende, Kakanui, New Zealand (USNM 143965); augite, Kakanui, New Zealand (USNM  
194 122142; Jarosewich et al. (1980), and glasses: rhyolite from Yellowstone, USA (Nash 1992)  
195 and Ja-rhyolite (USNM72857 VG-568; Jarosewich et al. 1980).

196

### 197 **Crystal size distribution analysis**

198 Crystal size distribution (CSD) analyses of plagioclase, amphibole or pyroxene were  
199 performed using back-scattered electron (BSE) images acquired with the electron microprobe.  
200 The analysis consisted of the measurement of two-dimensional parameters corresponding to  
201 the longer axis and the orthogonal short axis (length and width respectively) of each crystal  
202 using the open source computer program *ImageJ* (Schneider et al. 2012;  
203 <http://imagej.nih.gov/ij/>). For the characterization of the crystal sizes, at least seven BSE  
204 pictures at the same magnifications (1600X, 800X or 400X) were analyzed for each sample.  
205 The magnifications were chosen based on the average size and number of crystals to ensure

206 that a minimum of 90 crystals could be measured for each experiment. The magnifications  
207 translate to sample area per image of  $0.27 \text{ mm}^2$  (400X) and  $0.02 \text{ mm}^2$  (1600X). The crystal  
208 size measurement was manual and each crystal in the image was measured individually. The  
209 data (length and width) were used to calculate the approximate area of the surface of each  
210 crystal, their frequency distribution, crystal area fraction ( $\phi$ ) and crystal number density. The  
211 crystal number density ( $N_A$ ) is the frequency, for each size interval (bins), divided by the total  
212 area measured (Higgins 2000) while the crystal surface area was calculated by multiplying  
213 length and width and was used to obtain crystal area fraction. The crystal area fraction was  
214 calculated by dividing the total crystal area by the total area measured. The  $\phi$  and  $N_A$  were  
215 then used to calculate a characteristic crystal size ( $S_N = (\phi/N_A)^{0.5}$ ) and volume crystal density  
216 ( $N_V = N_A / S_N$ ) (Blundy and Cashman 2008).  
217 The number of crystals analyzed per photo mosaic was variable: plagioclase from 210 to  
218 2017; amphibole from 115 to 605; and pyroxene from 98 to 370. In all experimental samples,  
219 amphibole or pyroxene crystals have lower crystal number densities than plagioclase.

220

## 221 **Experimental results**

### 222 **Dry powder vs. pre-hydrated melt**

223 Plagioclase and pyroxene were used for two-dimension crystal size analyses for experiments  
224 performed at 1 kbar while plagioclase and amphibole were used for experiments performed at  
225 2 kbar (their compositions can be found in Supplementary Datasets B, C and D). All  
226 experiments with pre-hydrated glass as starting material (Ex11, Ex13 at 1 kbar and Ex44 at 2  
227 kbar; Fig. 1) have larger plagioclase (Figs. 2A and 3A), pyroxene (Figs. 2B) or amphibole  
228 crystals (Fig. 3B) than those found in experiments with dry glass and H<sub>2</sub>O as starting material  
229 (Ex12 and Ex14 at 1 kbar and Ex45 at 2 kbar).

230 At 1 kbar, when we compare crystal sizes in the runs in which temperature was kept constant  
231 (Ex11 and Ex12), we observe that the experiment with pre-hydrated glass (Ex11) exhibits  
232 plagioclase and pyroxene crystals up to a maximum of four times larger than those found in  
233 the experiment where dry glass and water was used (Ex12) (Figs. 2A and 2B). In experiments  
234 where temperature was cycled (Ex13 and Ex 14) plagioclase and pyroxene are only slightly  
235 larger in the pre-hydrated experiments (Ex13) than in experiments with dry glass plus water  
236 (Ex14) (Supplementary Dataset E). Similar crystal size distributions are observed in  
237 experiments performed at 2 kbar. Plagioclase and amphibole present a maximum crystal size  
238 up to two times larger in the experiments performed with pre-hydrated starting material  
239 (Ex44) than in the one with dry glass (Ex45) (Fig. 3A and 3B).

240 In experiments performed at static temperature, we observe that in the charges with dry glass  
241 and water (Ex12 and Ex45) plagioclase and pyroxene are respectively 50% to 90% and 20%  
242 to 30% more abundant in number of crystals than in experiments where pre-hydrated starting  
243 material (Ex14 and Ex44) was used, considering the same area. For experiments in which  
244 temperature was cycled, we observe that only the number of plagioclase crystals was more  
245 abundant using dry glass rather than pre-hydrated starting material. In contrast, the pyroxene  
246 crystal number was found to be lower.

247 Qualitative analyses of crystal morphology (Lofgren, 1974) show that plagioclase crystal  
248 shape was strongly affected by changing the nature of the starting material. In runs performed  
249 with pre-hydrated glass, skeletal crystals dominate. In contrast, when dry starting material and  
250 water was used tabular crystals prevail (see Figs. 4 and 5).

251 Concerning mineral compositions, no chemical zoning was observed in plagioclase, pyroxene  
252 or amphibole crystals in Ex11, Ex12, Ex13, Ex14 (1 kbar) and in Ex44, Ex45 (2 kbar).  
253 However, a significant variability of the plagioclase An (anorthite) content is observed  
254 between crystals of individual experiments (see Supplementary Dataset A; Fig. 6). This  
255 variability is usually larger for experiments performed on dry glass plus water than on pre-

256 hydrated glass. Pyroxene compositions equivalent in Ex13 and Ex14, while in Ex12 this  
257 mineral is slightly enriched in Fe in comparison to Ex11 (Fig. 7). Amphibole composition  
258 also present small variation between experiments and Ex44 shows higher amphibole Mg  
259 number  $[Mg/(MA+Fe^{2+})]$  than Ex45 (see Supplementary Dataset B; Fig. 8). Residual melt  
260 composition present small variability with Ex11 (pre-hydrated; 1 kbar), Ex14 (dry glass; 1)  
261 and Ex45 (dry glass; 2 kbar) showing higher  $Na_2O$  than Ex12 (dry glass; 1), Ex13 (pre-  
262 hydrated; 1 kbar), and Ex44 (pre-hydrated; 2 kbar). In addition, Ex14 exhibits higher  $K_2O$   
263 content than Ex13 (Table 3).

264

### 265 **1 kbar vs. 2 kbar experiments**

266 At 1 kbar orthopyroxene is the dominant mafic phase but amphibole and biotite are observed  
267 in experiments performed at 2 kbar. Plagioclase, ilmenite and magnetite were identified at  
268 both pressures. Plagioclase is the only mineral that can be used to estimate the effect of  
269 pressure on crystal sizes. Experiments performed at 2 kbar (Ex30 and Ex43) produced larger  
270 crystals than experiments performed at 1 kbar (Ex12 and Ex14). When dry starting material  
271 was used under static temperature, the maximum size of plagioclase crystals was up to three  
272 times larger in the 2 kbar experiment (Ex30) than in the 1 kbar experiment (Ex12) (Fig. 9A).  
273 When temperature was cycled, the maximum size of plagioclase crystals was up to five times  
274 larger at 2 kbar (Ex43) than at 1 kbar (Ex14) (Fig. 9B).

275 Regardless of the temperature path (cycling vs. static temperature), experiments at 2 kbar  
276 exhibit a lower plagioclase density than experiments at 1 kbar. For experiments with  
277 temperature cycling, considering the same area, Ex14 (1 kbar) has 99% more plagioclase  
278 crystals in number than Ex43 (2 kbar). For experiments at constant temperature, Ex12 (1  
279 kbar) exhibits only 6% more plagioclase crystals than Ex30 (2 kbar). No change of crystal  
280 morphology is observed by changing pressure, and plagioclase at 2 kbar is more enriched in  
281 An-component compared to plagioclase at 1 kbar (Fig. 6). A slight change of residual melt

282 composition is observed when comparing experiments at 2 kbar (Ex30 and Ex43) and 1 kbar  
283 (Ex12 and Ex14) with higher Al<sub>2</sub>O<sub>3</sub>, CaO, Na<sub>2</sub>O and lower K<sub>2</sub>O content at high pressure (Tab.  
284 3).

285

### 286 **Constant temperature vs. temperature cycling**

287 *1 kbar experiments* – Crystal size analyses were performed for plagioclase and pyroxene.  
288 Comparing experiments performed with dry glass plus 7% of water, the experiment at static  
289 temperature (Ex12) with very small plagioclase crystals ( $\leq 3 \mu\text{m}^2$ ) presents a higher crystal  
290 number density than the experiment in which temperature was cycled (Ex14) (Fig. 10A).  
291 However, both experiments show a similar crystal number density of large plagioclase  
292 crystals ( $\sim 13 \mu\text{m}^2$ ) with Ex14 having slightly larger plagioclase crystals than Ex12 (Fig. 10A).  
293 For pyroxene, temperature cycling did not effectively influence crystal growth and the static  
294 experiment (Ex12) resulted in larger crystals than the cycled one (Ex14) (Fig. 10B). Based on  
295 analyses of BSE images, we conclude that, considering the same area, Ex12 (constant  
296 temperature) displays  $\sim 24\%$  more plagioclase and  $\sim 17\%$  more pyroxene (Fig. 4) crystals than  
297 Ex14 (cycled temperature).

298 When pre-hydrated starting material is used, experiments with temperature cycling (Ex13 and  
299 Ex46) exhibit higher crystal number density of small plagioclase crystals than the static ones  
300 (Ex9 and Ex11) (Fig. 10A). For pyroxene, the experiment with temperature cycling performed  
301 at 775°C (Ex13) presents higher crystal number density of small crystals ( $\leq 3 \mu\text{m}^2$ ) than the  
302 static one (Ex11) (Fig. 10B). However, in the experiment performed at 815°C the static  
303 experiment (Ex9) presents a slightly higher crystal number density of small crystals ( $\leq 3$   
304  $\mu\text{m}^2$ ) than the one with temperature cycling (Ex46) (Supplementary Dataset F). All static  
305 experiments resulted in larger plagioclase and pyroxene crystals than the cycled ones. In  
306 terms of crystal fractions, BSE image analyses show that considering the same area, the  
307 cycling experiment with dry powder (Ex13) contains, in number of crystals,  $\sim 89\%$  more

12

308 plagioclase and ~67% more pyroxene crystals than the corresponding static one (Ex11) while  
309 Ex46 (cycling; pre-hydrated melt) contains ~66% more plagioclase and ~17% less pyroxene  
310 crystals than the static one (Ex9). No changes in crystal morphology are observed when only  
311 the temperature oscillation is taken into account (Fig. 4).

312 Plagioclase from experiments using pre-hydrated starting material and temperature cycling  
313 (Ex13 and Ex46) show a smaller An range than plagioclases from experiments at constant  
314 temperatures (Ex11 and Ex9). In contrast, when dry glass and water is used, the plagioclase  
315 from the experiment at constant temperature (Ex14) exhibits a larger variation in An-content  
316 than its conjugate run with cycling temperature (Ex12) (Fig. 6). Pyroxene shows a very  
317 homogenous composition within individual samples but small compositional differences are  
318 observed between static and cycling experiments (Fig. 7).

319 Normalized glass composition values do not show significant differences between the 815°C  
320 experiments (Ex9-Ex46). For the 775°C experiments (Ex11 and Ex13), glass composition in  
321 Ex11 is slightly more enriched in Al<sub>2</sub>O<sub>3</sub>, FeO, CaO and Na<sub>2</sub>O than Ex13, at the expense of  
322 SiO<sub>2</sub> (Table 3).

323

324 **2 kbar experiments** – Under this condition plagioclase and amphibole were the phases used  
325 for crystal size analyses. Experiments with temperature cycling show consistently larger  
326 plagioclase crystals than the static ones (Fig. 11A). For amphibole, we obtained contrasting  
327 results. When dry starting material was used the largest amphibole crystals in cycling  
328 experiments are approximately four times larger than those of static experiments (Fig. 11B).  
329 When pre-hydrated starting material was used amphibole is slightly larger in experiments at  
330 constant temperature (Fig. 11B). However, in experiments performed at 725°C, temperature  
331 cycling (Ex21) resulted in a higher concentration of very small amphibole crystals ( $\leq 3 \mu\text{m}^2$ )  
332 than at static temperature (Ex44), while in experiments performed at 750°C we observe the  
333 opposite.

334 In terms of number of crystals, experiments performed with static temperature always contain  
335 more crystals than experiments performed with cycled temperature (Figs. 4 and 5). In most of  
336 the experiments the morphology of plagioclase did not change when using temperature  
337 cycling. However, in Ex22 (dry glass plus water) we observe the occurrence of tabular and  
338 skeletal crystals while the corresponding static experiment (Ex45) only shows tabular crystals.  
339 Plagioclase crystals do not display chemical zoning in most experiments performed at 2 kbar  
340 with the exception of two charges (Ex20 and Ex21), with a compositional zoning varying  
341 from ~38 mol% (core) to 32-34 mol% (rim) in An content. In addition to zoning, plagioclase  
342 exhibits a significant compositional range of An within a single charge, with Ex15 (static  
343 temperature) showing the largest range of An-content (An<sub>33</sub> to An<sub>48</sub>) of all experiments  
344 performed at 2 kbar (Fig. 6). No significant compositional variability was observed in  
345 amphibole in individual experiments, with the exception of Ex43, but the amphibole Mg  
346 number [Mg/(Mg+Fe<sup>2+</sup>)] varies between experiments (Fig. 8). Melt compositions vary  
347 slightly between cycling and static experiments. Ex21 and Ex22 (cycling temperature) exhibit  
348 higher Na<sub>2</sub>O and K<sub>2</sub>O than Ex44 and Ex45, while Ex15 (static temperature) presents higher  
349 Na<sub>2</sub>O and K<sub>2</sub>O than Ex20 (cycling temperature) (Table 3).

350

351

## Discussion

### Attainment of equilibrium

353 Reaching complete equilibrium between crystals and melt is difficult in experimental  
354 petrology, and even more so at low temperatures (700 to 800°C) for highly polymerized melts  
355 (high Si content). To reach near-equilibrium conditions in these situations, long run duration  
356 experiments (weeks to a month) and homogenous starting materials are required. In this study,  
357 we performed experiments with a run duration of 14 to 21 days using crushed homogenous  
358 glass as starting material and under water-saturated conditions, which should facilitate the  
359 attainment of equilibrium.

360 Classical evidences for equilibrium as mentioned in the literature are and identified in our  
361 experiments are: (1) euhedral crystal shapes, without inclusions and evenly distributed  
362 throughout the gold capsules and (2) chemically unzoned crystals, as well as homogeneous  
363 melt composition. In our study, plagioclase crystals are usually euhedral, evenly distributed  
364 throughout the capsules and unzoned in most of the experiments with exception of four runs  
365 performed with pre-hydrated starting material (Ex9 and Ex46 at 1 kbar, and Ex20 and Ex21 at  
366 2 kbar). However, when crystals from different locations within a single charge are analyzed,  
367 they can present significant variations in anorthite content. The largest An range was observed  
368 in Ex15 where plagioclase crystals show an An content ranging between An<sub>33</sub> to An<sub>48</sub>. This  
369 relatively large compositional variation can be observed in many studies of phase equilibria in  
370 felsic systems (e.g., Scaillet et al., 1995). However, in such studies, only few plagioclase  
371 crystals from each experiment were usually analyzed, in contrast to the systematic in this  
372 study. Previous studies interpreted the variation of plagioclase An-content within individual  
373 experiments to be caused by heterogeneous distribution of water at the beginning of  
374 experiments, where the more calcic plagioclase crystallized before the water-melt equilibrium  
375 was attained (Scaillet & Evans 1999; Costa 2004). However, this explanation probably needs  
376 to be reconsidered, at least for the experiments in which pre-hydrated glasses were used as  
377 starting material. For example, in Ex15 which was conducted with pre-hydrated glass, the  
378 results may indicate that although plagioclase is not in complete equilibrium at the sample  
379 scale, local equilibrium was attained. Such local variations may be due to different  
380 crystallization rates of plagioclase and other Ca-bearing minerals such as amphibole. If  
381 amphibole crystallizes faster than plagioclase, the local environment of this mineral may be  
382 depleted in constituents forming amphibole, and plagioclase growing in the vicinity may  
383 record this local change of melt composition (e.g., Pichavant et al. 2007).

384 In two charges (Ex20 and Ex21) a few plagioclase crystals show zoning with a relatively large  
385 variation in An content between the core (37-38 mol% An) and the rim (31-34 mol% An).

386 Both experiments were performed with temperature cycling and pre-hydrated starting  
387 material. The zoned plagioclase crystals were usually larger than the average minerals. We  
388 speculate that diffusion in pre-hydrated glass is faster than in dry glass in the first hours of  
389 experiments which helped crystal growth and consequently increased the chances of forming  
390 crystals with normal zoning.

391 We carried out an additional test to evaluate equilibrium conditions comparing the glass and  
392 mineral compositions of experiments performed at the same pressure and temperature. We  
393 observed that experiments run in the same vessel are similar in composition, while  
394 experiments run in separate vessels at the same P and T conditions may present variations in  
395 Fe and Mg content. For example, Ex11 and 12 were run together at constant T in a new vessel  
396 of the laboratory while, Ex13 and Ex14 (cycling T) were run in one of the oldest vessels. We  
397 assigned the difference in Fe and Mg content between one set of experiments and the other to  
398 possible differences in  $fO_2$  prevailing in the vessels, independently of temperature cycling.  
399 The CSPVs are made of a Ni-based alloy and therefore, the intrinsic  $fO_2$  may change.  
400 According to the results presented here, with pyroxenes from the older vessel showing higher  
401 Mg and lower Fe content than those from the newer vessel, we assume that the intrinsic  $fO_2$   
402 becomes slightly more oxidizing with time.

403

#### 404 **The effect of starting material on crystal phases**

405 The experiment pairs conducted either at static temperature or with cycling temperature lead  
406 to the same conclusions: (1) we observe the same mineral assemblages, and no systematic  
407 change in mineral compositions between experiments performed with pre-hydrated glass and  
408 dry glass. This means that the starting material does not influence phase relationships or  
409 compositions; (2) most experiments conducted with pre-hydrated glass have larger and less  
410 crystals than experiments conducted with dry powder. One possible explanation to this  
411 observation is that the absence of fluid between the grains of the starting powder and the

412 homogeneous distribution of volatiles in the pre-hydrated starting glasses contribute to  
413 reducing the nucleation of phases along grain boundaries during the initial stages of the  
414 experiment. This observation also implies that fluid-absent experiments can be conducted at a  
415 water activity which is controlled very accurately if pre-hydrated glasses with well-  
416 characterized water concentrations are used. However, it should be noted that all strongly  
417 zoned plagioclase crystals identified in this study are in experiments performed using pre-  
418 hydrated starting material; (3) a possible inconvenience of using pre-hydrated starting  
419 material is its strong effect on plagioclase crystal morphology. Skeletal, anhedral crystals with  
420 rough surface are more common in such experiments than in those performed with a dry  
421 glass.

422 Previous experimental studies demonstrated that plagioclase crystal morphology is strongly  
423 dependent on the degree of supercooling (Lofgren, 1974; Corrigan, 1982). They showed that  
424 the shape of plagioclase changes from tabular to skeletal with formation of dendrites and  
425 spherulites when cooling rate increases. However, we obtained changes in plagioclase crystal  
426 morphology from experiments with identical cooling rates, when we used a pre-hydrated  
427 starting material (see Fig. 4 (Ex11 vs. Ex12); (Ex13 vs. Ex14) and Fig. 5 (Ex44 vs. Ex21)).  
428 We speculate that a change of the dominant process of crystal growth occurs from interface-  
429 controlled when dry glass plus water is used to diffusion-controlled when pre-hydrated  
430 starting material is used. Interface-controlled growth leads to planar, faceted morphology and  
431 smooth surface (Kirkpatrick, 1975) while diffusion-controlled growth leads to cellular  
432 morphology and skeletal shapes (Kirkpatrick, 1975; Hammer, 2008).

433

#### 434 **The effect of pressure on crystal phases**

435 As already noted in several studies, variation of P in the range of 1 - 2 kbar can have a strong  
436 effect on the stability of mafic phases. The mineral assemblage formed at 1 kbar is made up of  
437 plagioclase, orthopyroxene, magnetite and ilmenite, while in 2 kbar experiments the

438 assemblage is integrated by plagioclase, amphibole, biotite, magnetite and ilmenite. Thus, this  
439 study confirms that hydrous minerals such as amphibole and biotite are not stable at low  
440 pressure when the water content of the melt is close to or below 4 wt% H<sub>2</sub>O (e.g., Rutherford  
441 and Hill 1993; Venezky and Rutherford 1999; Cichy et al. 2011).

442 Interestingly, temperature cycling ( $\pm 15^{\circ}\text{C}$ ) at 2 kbar increased plagioclase crystal size, while  
443 at 1 kbar we observed the opposite effect. These differences are interpreted as being due to  
444 properties of the silicate melt such as viscosity and diffusivity that are influenced, among  
445 other parameters, (e.g. degree of polymerization and temperature) by the amount of water  
446 dissolved in the melt. As our experiments were conducted at nearly water-saturated  
447 conditions, one major difference between 1 and 2 kbar runs is that the water content in the  
448 melt was in the range of 3.5 - 4 wt% H<sub>2</sub>O at 1 kbar and between 6 - 6.5 wt% H<sub>2</sub>O at 2 kbar.

449 Assuming that small changes in temperature ( $25^{\circ}\text{C}$ ) do not affect water solubility significantly  
450 (Holtz et al. 1995) and using the models of water solubility from Behrens and Jantos (2001)  
451 and the the model of Hess and Dingwell (1996) for calculation of viscosity, we calculate that  
452 the melt viscosity in our experiments performed at 1 and 2 kbar is of  $10^{5.3}$  and  $10^{4.6}$  Pa.s,  
453 respectively. Additionally, at 1 kbar, orthopyroxene (Ca-free phase) dissolved at high  
454 temperature and crystallized at low temperature together with plagioclase, while at 2 kbar,  
455 amphibole (Ca-bearing phase) was the mineral affected. This change in Ca concentration in  
456 the melt with temperature cycling will be different in the 1 and 2 kbar experiments, possibly  
457 affecting the kinetics of dissolution and growth of plagioclase.

458

#### 459 **The effect of temperature cycling on crystal phases**

460 **Experiments performed at 1 kbar.** One possible explanation for the small effect of  
461 temperature cycling on the crystal size at 1 kbar may be that the cycling amplitude chosen  
462 ( $\pm 15^{\circ}\text{C}$ ) was not high enough to completely dissolve the small crystals during the high  
463 temperature interval. In one series of experiments, the experiment in which the temperature

464 was cycled not only has smaller crystals, but also presents a higher crystal number density  
465 than the counterpart experiment in which temperature was constant (see Fig. 3A and Fig. 3B).  
466 This observation could indicate that new nuclei, together with the growth of crystals that  
467 survived dissolution at high temperature, formed when temperature decreased. As a  
468 consequence, the overall crystal number density increased and the crystal size decreased. The  
469 results observed in experiments at 815 ( $\pm 15^\circ\text{C}$ ) corroborate this interpretation, since the  
470 minerals exhibit less prominent size differences than those in the experiments performed at  
471  $775^\circ\text{C}$  ( $\pm 15^\circ\text{C}$ ). We also observed that in the experiments performed at  $775^\circ\text{C}$  ( $\pm 15^\circ\text{C}$ ) the  
472 largest plagioclase and pyroxene crystals are  $\sim 3$  times larger in the static experiments (Fig.  
473 3A). At  $815^\circ\text{C}$  ( $\pm 15^\circ\text{C}$ ) the largest plagioclase is only  $\sim 2$  times larger (Fig. 6A) and  
474 pyroxene just slightly larger (Fig. 6B) in static than in cycling experiments. We speculate that  
475 at the high temperature stage of  $815^\circ\text{C} \pm 15^\circ\text{C}$  ( $830^\circ\text{C}$ ) experiments, the conditions are closer  
476 to the liquidus temperature of pyroxene and therefore small crystals start to completely  
477 dissolve.

478 Mills & Glazner (2013) demonstrated that at atmospheric pressure, the amplitude is one of the  
479 major parameters that directly control the degree of crystal coarsening. Our results show that  
480 for a highly polymerized starting material at 1 kbar and temperature of  $\leq 815^\circ\text{C}$ , the  
481 amplitude of  $\pm 15^\circ\text{C}$  will not increase the crystal size. However, at the same conditions, pre-  
482 hydrated starting material at constant temperature does indeed significantly increase crystal  
483 size.

484 **Experiments performed at 2 kbar.** A large difference in the amount (number of  
485 crystals considering the same surface area) of plagioclase and amphibole crystals was  
486 observed between Ex30 ( $775^\circ\text{C}$ ) and Ex43 ( $775 \pm 15^\circ\text{C}$ ). Ex30 has  $\sim 99\%$  more plagioclase  
487 crystals and  $\sim 89\%$  more amphibole crystals than Ex43. Approximately 97% of plagioclase  
488 crystals in Ex30 (constant T) have a surface area of  $\leq 0.00001 \text{ mm}^2$  while the smallest  
489 plagioclase crystal in Ex43 (cycling) has an area of  $0.00005 \text{ mm}^2$ . A possible explanation for

490 this difference in crystal size and proportion is that with a temperature of 775°C and a cycling  
491 amplitude of  $\pm 15^\circ\text{C}$ , the maximum temperature reaches 790°C. The textures observed in Ex43  
492 (Fig. 7) have lower crystal densities and larger and cleaner melt pools than other experiments,  
493 indicating that this sample is close to liquidus temperature, therefore resulting in improved  
494 dissolution of small crystals at the peak temperature and a smaller crystal number density.

495

496

### Implications

497 This study shows that the best approach to increase plagioclase, pyroxene or amphibole  
498 crystal sizes in crystallization experiments performed from highly polymerized melts, under  
499 water-saturated conditions and at low temperatures (700°C – 800°C) is to use pre-hydrated  
500 glass as starting material. However, the formation of zoned plagioclase crystals seems to be  
501 favored by using pre-hydrated glass.

502 The effect of temperature cycling on crystal size changes between experiments at 1 kbar and  
503 those performed at 2 kbar. Our explanation for this different behavior is that temperature  
504 cycling is more effective if melt viscosities and cation diffusivities are low, which increases  
505 the kinetics of crystal growth and dissolution. The temperature amplitude of cycling is also  
506 important and cycling may have strong or minor effects, depending on the amount of phases  
507 present during the high temperature stage of the temperature path. Finally, our methodological  
508 study of crystallization processes indicates that the composition of plagioclase can vary by  
509 nearly 10 mol% within one experiment, which may be due to small local compositional  
510 variations related to the crystallization of other neighbor phases. This compositional range is  
511 slightly lower in experiments with cycling temperature than in experiments performed at  
512 static temperature (Fig. 6).

513

514

515

516

## Acknowledgements

517 We would like to thank the head of the workshop at the Institute for Mineralogy at Leibniz  
518 University Hannover, Ulrich Kroll, for technical support and Julian Feige for sample  
519 preparation. Further thanks go to Eric Wolff and Chao Zhang for analytical support and to  
520 Adriana Currin for language revision. We also would like to thank the editor Charles Lesher,  
521 as well as the reviewers Julia Hammer and Ryan D. Mills for their comments and suggestions  
522 that helped improve the manuscript. This work was funded by the DAAD and CNPq  
523 (fellowship to the first author) and the Deutsche Forschungsgemeinschaft (DFG; project  
524 HO1337/31 in the frame of the ICDP program). Olivier Namur acknowledges support from an  
525 Emmy Noether program from the DFG.

526

## REFERENCES CITED

- 528 Behrens, H., Roman, C., Nowak, M., and Holtz, F. (1996) Near-infrared spectroscopic determination of water  
529 species in glasses of the system MAISi<sub>3</sub>O<sub>8</sub> (M = Li, Na, K): an interlaboratory study, 2541.  
530 Behrens, H., and Jantos, N. (2001) The effect of anhydrous composition on water solubility in granitic melts.  
531 American Mineralogist, 86, 14–20.  
532 Blundy, J., and Cashman, K. (2008) Petrologic Reconstruction of Magmatic System Variables and Processes.  
533 Reviews in Mineralogy and Geochemistry, 69, 179–239.  
534 Charlier, B., and Grove, T.L. (2012) Experiments on liquid immiscibility along tholeiitic liquid lines of descent.  
535 Contributions to Mineralogy and Petrology, 164, 27–44.  
536 Cichy, S.B., Botcharnikov, R.E., Holtz F., and Behrens, H. (2011) Vesiculation and Microlite Crystallization in  
537 the ascending rhyodacitic magma of the 1991-95 Eruption of Unzen Volcano. Japan Journal of  
538 Petrology, 52, 1469-1492.  
539 Corrigan, G.M. (1982) The crystal morphology of plagioclase feldspar produced during isothermal supercooling  
540 and constant rate cooling experiments. Mineralogical Magazine, 46, 433–439.  
541 Costa, F. (2004) Petrological and experimental constraints on the pre-eruption conditions of holocene dacite  
542 from volcan San Pedro (36 S, Chilean Andes) and the importance of sulphur in silicic subduction-  
543 related magmas. Journal of Petrology, 45, 855–881.  
544 Erdman, M., and Koepke, J. (2016) Experimental temperature cycling as a powerful tool to enlarge melt pools  
545 and crystals at magma storage conditions. American Mineralogist, 101, 960–969.  
546 Fenn, P. (1977). The Nucleation and Growth of Alkali Feldspars From Hydrous Melts. The Canadian  
547 Mineralogist, v. 15, p. 135–161.  
548 Gardner, J.E., Rutherford, M., Carey, S., and Sigurdsson, H. (1995) Experimental constraints on pre-eruptive  
549 water contents and changing magma storage prior to explosive eruptions of Mount St Helens volcano.  
550 Bulletin of Volcanology, 57, 1–17.  
551 Hammer, J.E. (2008) Experimental Studies of the Kinetics and Energetics of Magma Crystallization. Reviews in  
552 Mineralogy and Geochemistry, 69, 9–59.  
553 Hess, K.U., and Dingwell, D.B. (1996) Viscosities of hydrous leucogranitic melts: a non-Arrhenian model.  
554 American Mineralogist, 81, 1297–1300.  
555 Higgins, M.D. (2000) Measurement of crystal size distributions. American Mineralogist, 85, 1105–1116.  
556 Holtz, F., Pichavant, M., Barbey, P., and Johannes, W. (1992) Effects of H<sub>2</sub>O on liquidus phase relations in the  
557 haplogranitic system at 2 and 5 kbar. American Mineralogist, 77, 1223-1241.  
558 Holtz, F., Behrens, H., Dingwell, D.B., and Johannes W. (1995) Water solubility in haplogranitic melts.  
559 Compositional, pressure and temperature dependence. American Mineralogist, 80, 94-108.  
560 James, R.S., and Hamilton, D.L. (1969) Phase relations in the system NaAlSi<sub>3</sub>O<sub>8</sub>-KAlSi<sub>3</sub>O<sub>8</sub>-CaAl<sub>2</sub>Si<sub>2</sub>O<sub>8</sub>-SiO<sub>2</sub> at  
561 1 kilobar water vapour pressure. Contributions to Mineralogy and Petrology, 21, 111-141.  
562 Jarosewich, E., Nelen, J.A, and Norberg, J.A. (1980) Reference samples for electron microprobe and scanning  
563 electron micropobe analyses. Geostandards Newsletter, 4, 43-47.  
564 Kirkpatrick, R.J. (1975) Crystal Growth from the Melt : A Review. Am. Mineral., 60, 798–814.  
565 Lofgren, G. (1974). An Experimental Study of Plagioclase Crystal Morphology: Isothermal Crystallization  
566 American Journal of Science.  
567 Mills, R.D., and Glazner, A.F. (2013) Experimental study on the effects of temperature cycling on coarsening of  
568 plagioclase and olivine in an alkali basalt. Contributions to Mineralogy and Petrology, 166, 97–111.  
569 Nandedkar, R.H., Ulmer, P., and Müntener, O. (2014) Fractional crystallization of primitive, hydrous arc  
570 magmas: an experimental study at 0.7 GPa. Contributions to Mineralogy and Petrology, 167, 1–27.  
571 Nash, W.P. (1992) Analysis of oxygen with the electron micropobe: applications to hydrated glasses and  
572 minerals. American Mineralogist, 77, 453-7.  
573 Pichavant, M. (1987) Effects of B and H<sub>2</sub>O on liquidus phase relations in the haplogranite system at 1 Kbar.  
574 American Mineralogist, 72, 1056-1070.  
575 Pichavant, M. Costa, F., Burgisser, A., Scaillet, B., M.C, and Poussineau, S. (2007) Equilibration scales in silicic  
576 to intermediate magmas. Implications for experimental studies. Journal of Petrology, 00, 1-18  
577 Patiño Douce, A.E., and Beard, J.S (1996) Effects of P, f(O<sub>2</sub>) and Mg/Fe ratio on dehydration melting of model  
578 metagreywackes. Journal of petrology, 37, 999-1024.  
579 Patino Douce, A.E., and Harris, N. (1998) Experimental constraints on Himalayan anatexis. Journal of petrology,

- 580 39, 689-710.
- 581 Rushmer, T. (1995) An experimental deformation study of partially molten amphibolite—application to low-  
582 melt fraction segregation. *Journal of Geophysical Research*, 100, 15681–15695.
- 583 Rutherford, M.J., and Hill, P.M. (1993). Magma ascent rates from amphibole breakdown: an experimental study  
584 applied to the 1980-1986 Mount St. Helens eruption. *Journal of Geophysical Research*, 98, 19667-  
585 19685.
- 586 Scaillet, B., and Evans, B.W. (1999) The 15 June 1991 eruption of Mount Pinatubo. I. Phase equilibria and pre-  
587 eruption P–T– $f_{O_2}$ – $f_{H_2O}$  conditions of the dacite magma. *Journal of Petrology*, 40, 381–411.
- 588 Scaillet, B., Pichavant, M., and Roux, J. (1995) Experimental crystallization of Leucogranite Magmas. *Journal of*  
589 *Petrology*, 36, 663-705.
- 590 Scaillet, B. Holtz, F., and Pichavant, M. (2016) Experimental constraints on the formation of silicic magmas.  
591 *Elements*, 12, 109-114. doi: 10.2110/gelements.12.2.109 .
- 592 Schneider, C.A., Rasband, W.S., and Eliceiri, K.W. (2012) NIH Image to *ImageJ*: 25 years of image analysis.  
593 *Nature* 445 Methods, 9, 671-675.
- 594 Shea, T.; Hammer, J. E. (2013). Oxidation in CSPV experiments involving H<sub>2</sub>O-bearing mafic magmas:  
595 Quantification and mitigation. *American Mineralogist*, v. 98, n. 7, p. 1285–1296.
- 596 Tuttle, O.F., and Bowen, N.L. (1958) Origin of granite in light of experimental studies in the system  
597 NaAlSi<sub>3</sub>O<sub>8</sub>-KAlSi<sub>3</sub>O<sub>8</sub>-SiO<sub>2</sub>-H<sub>2</sub>O. *Geological Society of America Memoir*, 74, 145 p.
- 598 Venezky, D.Y., and Rutherford, M.J. (1999) Petrology and FeTi oxide reequilibration of the 1991 Mount Unzen  
599 mixed magma. *Journal of Volcanology and Geothermal Research* 89, 212–230.
- 600

601

## Figure captions

602 **Figure 1.** Flow-chart of the experimental strategy.

603

604 **Figure 2.** Log-plot of crystal and population number density vs. square root of plagioclase  
605 ( $N_A^{\text{plag}}$ ) and pyroxene ( $N_A^{\text{pyr}}$ ) surface area for Ex12 and Ex11. This figure illustrates the effect  
606 of starting material on crystal size and on crystal number density. We observe that pre-  
607 hydrated starting material greatly increases plagioclase (A) and pyroxene (B) crystal sizes.  
608 Experiments performed with dry glass exhibit higher crystal number density of smaller  
609 plagioclase and pyroxene crystals. Circles represent area number density ( $N_A$ ,  $\text{mm}^{-2}$ ) and  
610 squares represent population number density ( $N_v$ ,  $\text{mm}^{-3}$ ).

611

612 **Figure 3.** Log-plot of crystal and population number density of plagioclase ( $N_A^{\text{plag}}$ ) and  
613 amphibole ( $N_A^{\text{amph}}$ ) vs. the square root of the mineral surface area for Ex45 and Ex44. At 2  
614 kbar experiments performed with pre-hydrated starting material (Ex44) also present larger  
615 plagioclase (A) and amphibole (B) crystals than those performed with dry glass (Ex44). In  
616 addition, the experiment with dry glass (Ex45) exhibits a higher crystal number density than  
617 the pre-hydrated experiment (Ex44). Circles represent area number density ( $N_A$ ,  $\text{mm}^{-2}$ ) and  
618 squares represent population number density ( $N_v$ ,  $\text{mm}^{-3}$ ).

619

620 **Figure 4.** Backscattered electron images (BSE) (see table 2 for run details) of experiments  
621 performed at 1 kbar. The images show the differences in texture and in abundance of crystals  
622 of different experiments. P.H.: Pre-hydrated and D.G.: Dry glass. Phase abbreviation: Pl,  
623 plagioclase; OPX, orthopyroxene.

624

625 **Figure 5.** Backscattered electron (BSE) images (see table 2 for run details) of 2 kbar  
626 experiments showing the differences in texture and crystal abundance between experiments  
627 performed under constant or cycling temperature. P.H.: Pre-hydrated and D.G.: Dry glass.  
628 Phase abbreviations: Pl, plagioclase; Amph, amphibole, Bt, biotite.

629

630 **Figure 6.** Ternary diagram of plagioclase composition. (A) Plagioclase chemical variation in  
631 experiments performed at 1 kbar and (B) plagioclase compositional variation of experiments  
632 performed and 2 kbar. Experiments performed at 2 kbar show a larger variation of An  
633 (anorthite) content than experiments performed at 1 kbar.

634

635 **Figure 7.** Ternary diagram of orthopyroxene for experiments performed at 1 kbar. Pyroxene  
636 crystals exhibit a homogenous composition within the same charge.

637

638 **Figure 8.** Amphibole compositional diagram for experiments performed at 2 kbar. Amphibole  
639 Mg number [ $\text{Mg}/(\text{Mg}+\text{Fe}^{2+})$ ] does not show a significant variation present within individual  
640 charges in almost all experiments with the exception of Ex43. It is however variable between  
641 experiments.

642

643 **Figure 9.** Log-plot of crystal and population number density of plagioclase ( $N_A^{\text{plag}}$ ) vs. the  
644 square root of the mineral area for Ex12 and Ex30, Ex14 and Ex43. Experiments performed at  
645 2 kbar present larger plagioclase crystals than those performed at 1 kbar. Circles represent  
646 area number density ( $N_A$ ,  $\text{mm}^{-2}$ ) and squares represent population number density ( $N_v$ ,  $\text{mm}^{-3}$ ).

647

648 **Figure 10.** Log-plot of crystal number density and population number density of plagioclase  
649 ( $N_A^{\text{plag}}$ ) and pyroxene ( $N_A^{\text{pyr}}$ ) vs. the square root of the mineral surface area. (A) Ex12  
650 presents a higher concentration of small plagioclase crystals ( $\leq 3 \mu\text{m}^2$ ) than Ex14, while both

651 experiments present very similar crystal number densities of the larger ( $\sim 13 \mu\text{m}^2$ ) crystals.  
652 Ex11 (static T) present larger plagioclase crystal number density than Ex13 (cycling T).  
653 (B) Ex12 and 11 (static T) presents larger pyroxene crystals than Ex14 and Ex13 (cycling).  
654 Circles represent area number density ( $N_A, \text{mm}^{-2}$ ) and squares represent population number  
655 density ( $N_v, \text{mm}^{-3}$ ).

656

657 **Figure 11.** Log-plot of the crystal number density of plagioclase ( $N_A^{\text{plag}}$ ) and amphibole  
658 ( $N_A^{\text{amph}}$ ) plotted against the square root of the mineral surface area for Ex21, Ex22, Ex44 and  
659 Ex45. (A) Ex21 and Ex22, performed with temperature cycling, presents larger plagioclase  
660 crystals than Ex 44 and Ex45 performed with static temperature. (B) Amphibole was greatly  
661 affected by temperature cycling when dry starting material was used and the largest  
662 amphibole crystal in Ex22 is  $\sim 4$  times larger than the largest crystal in E45. In another hand,  
663 when pre-hydrated starting material was used, amphibole is slight larger in the static T  
664 experiment (Ex44) in comparison with the cycling one (Ex21). The circles represent area  
665 number density ( $N_A, \text{mm}^{-2}$ ) and the squares represent population number density ( $N_v, \text{mm}^{-3}$ ).

666

667

**Table 1.** Starting composition (wt%)

Sample	Pre-hydrated starting material	Dry glass starting material
n: <sup>1</sup>	15	24
SiO <sub>2</sub>	70.83 <sup>4</sup> (0.45) <sup>3</sup>	70.63 (0.46)
TiO <sub>2</sub>	0.42 (0.03)	0.45 (0.04)
Al <sub>2</sub> O <sub>3</sub>	14.87 (0.23)	15.23 (0.50)
FeO	3.07 (0.17)	3.02 (0.20)
MnO	b.d <sup>2</sup>	b.d
MgO	0.93 (0.06)	1.01 (0.06)
CaO	2.71 (0.15)	2.83 (0.12)
Na <sub>2</sub> O	3.54 (0.23)	3.77 (0.23)
K <sub>2</sub> O	3.61 (0.09)	3.48 (0.12)
Total <sup>5</sup>	92.15	100.41

**Notes:** <sup>1</sup>Number of analyses

<sup>2</sup>Below detection limit

<sup>3</sup>Number in parentheses indicates one standard deviation of replicate analyses

<sup>4</sup>Pre-hydrated analyses values were normalized to 100%

<sup>5</sup>Original total

668

669

**Table 2.** Experimental conditions, durations and run products

Run	P [kbar]	P. H. <sup>2</sup> or D. G. <sup>3</sup>	T [°C]	Cycling or constant T	Duration [Days]	Results
Ex 11	1	P.H	775	constant	21	Pl, Opx, Ox
Ex 13	1	P.H	775± 15	cycling	21	Pl, Opx, Ox
Ex 12	1	D.G	775	constant	21	Pl, Opx, Ox
Ex14	1	D.G	775± 15	cycling	21	Pl, Opx, Ox
Ex 9	1	P.H	815	constant	21	Pl, Opx, Ox
Ex 46	1	P.H	815± 15	cycling	21	Pl, Opx, Ox
Ex 45	2	D.G	725	constant	21	Pl, Amph, Bt, Ox
Ex 22	2	D.G	725± 15	cycling	21	Pl, Amph, Bt, Ox
Ex 44	2	P.H	725	constant	21	Pl, Amph, Bt, Ox
Ex 21	2	P.H	725± 15	cycling	21	Pl, Amph, Bt, Ox
Ex 15	2	P.H	750	constant	21	Pl, Amph, Bt, Ox
Ex 20	2	P.H	750± 15	cycling	21	Pl, Amph, Bt, Ox
Ex 30	2	D.G	775	constant	14	Pl, Amph, Bt, Ox
Ex 43	2	D.G	775± 15	cycling	14	Pl, Amph, Bt, Ox

**Notes:** All experiments were run with 7 wt% of H<sub>2</sub>O contend

<sup>2</sup>Pre-hydrated starting material

<sup>3</sup>Dry starting material

Phase abbreviation: Pl, plagioclase; OPX, orthopyroxene; Amph, amphibole; Bt, biotite; Ox, oxides.

670

671

**Table 3.** Composition of residual melt

Run	Ex 11	Ex 13	Ex 12	Ex14	Ex 9	Ex 46	Ex 45	Ex 22	Ex 44	Ex 21	Ex 15	Ex 20	Ex 30	Ex 43
T [°C]	775	775 ±15	775	775 ±15	815	815 ±15	725	725 ±15	725	725 ±15	750	750 ±15	775	775 ±15
P [kbar]	1	1	1	1	1	1	2	2	2	2	2	2	2	2
n <sup>1</sup>	14	8	20	14	11	9	13	13	8	18	13	11	13	9
P. H <sup>2</sup> . or D. G <sup>3</sup>	P.H	P.H	D.G	D.G	P.H	P.H	D.G	D.G	P.H	P.H	P.H	P.H	D.G	D.G
SiO <sub>2</sub>	71.72 (0.69) <sup>4</sup>	74.18 (0.72)	70.94 (0.32)	72.58 (0.58)	71.16 (0.32)	71.24 (0.74)	70.57 (0.67)	72.69 (0.37)	71.59 (0.57)	72.34 (0.30)	68.88 (0.55)	71.37 (0.49)	69.12 (0.50)	68.04 (0.39)
TiO <sub>2</sub>	0.21 (0.03)	0.13 (0.03)	0.21 (0.04)	0.16 (0.02)	0.25 (0.03)	0.22 (0.03)	0.12 (0.06)	0.12 (0.04)	0.15 (0.05)	0.12 (0.04)	0.20 (0.04)	0.09 (0.04)	0.17 (0.06)	0.20 (0.02)
Al <sub>2</sub> O <sub>3</sub>	12.73 (0.22)	11.77 (0.27)	12.16 (0.28)	12.04 (0.23)	12.61 (0.23)	12.60 (0.24)	12.32 (0.36)	12.23 (0.26)	11.88 (0.25)	12.10 (0.14)	13.28 (0.08)	12.57 (0.18)	13.20 (0.25)	13.94 (0.34)
FeO	1.24 (0.22)	1.09 (0.31)	1.43 (0.20)	1.11 (0.31)	1.38 (0.12)	1.37 (0.22)	1.06 (0.31)	0.89 (0.15)	1.11 (0.38)	0.90 (0.05)	0.95 (0.20)	0.92 (0.16)	1.10 (0.25)	1.63 (0.22)
MnO	b.d <sup>5</sup>	b.d												
MgO	0.18 (0.05)	0.45 (0.20)	0.49(0.19)	0.59 (0.18)	0.22 (0.04)	0.40 (0.16)	0.63 (0.25)	0.16 (0.09)	0.30 (0.14)	0.18 (0.07)	0.49 (0.22)	0.15 (0.04)	0.61 (0.18)	0.65 (0.25)
CaO	1.09 (0.08)	0.96 (0.16)	1.17 (0.11)	0.96 (0.07)	1.19 (0.14)	1.23 (0.06)	1.37 (0.13)	1.22 (0.05)	1.28 (0.13)	1.24 (0.09)	1.73 (0.09)	1.36 (0.09)	1.63 (0.10)	1.83 (0.1)
Na <sub>2</sub> O	2.92 (0.23)	2.57 (0.39)	2.22 (0.46)	2.74 (0.16)	3.12 (0.34)	2.99 (0.17)	2.60 (0.17)	2.83 (0.11)	2.49 (0.22)	2.71 (0.11)	3.07 (0.18)	2.80 (0.15)	2.73 (0.10)	2.99 (0.09)
K <sub>2</sub> O	4.45 (0.12)	4.54 (0.16)	4.05 (0.17)	4.44 (0.08)	4.37 (0.15)	4.12 (0.11)	3.63 (0.10)	3.82 (0.11)	3.65 (0.11)	3.78 (0.06)	3.73 (0.15)	3.57 (0.12)	3.50 (0.07)	3.48 (0.13)
Total <sup>6</sup>	94.54	95.69	92.66	94.61	94.3	94.17	92.31	91.19	92.45	93.36	92.34	91.19	92.06	92.76

**Notes:** <sup>1</sup>Number of analyses

<sup>2</sup>Pre-hydrated starting material

<sup>3</sup>Dry starting material

<sup>4</sup>Number in parentheses indicate one standard deviation of replicate analyses

<sup>5</sup>Below detection limit

<sup>6</sup>Original total

# Figure 1

	Dry glass starting material plus H <sub>2</sub> O		Pre-hydrated starting material	
	1 kbar	2 kbar	1 kbar	2 kbar
725 °C		Ex22		Ex21
		Ex45		Ex44
750 °C				Ex20
				Ex15
775 °C	Ex14	Ex43	Ex13	
	Ex12	Ex30	Ex11	
815 °C			Ex46	
			Ex9	

 cycling T  
 static T

Figure 2

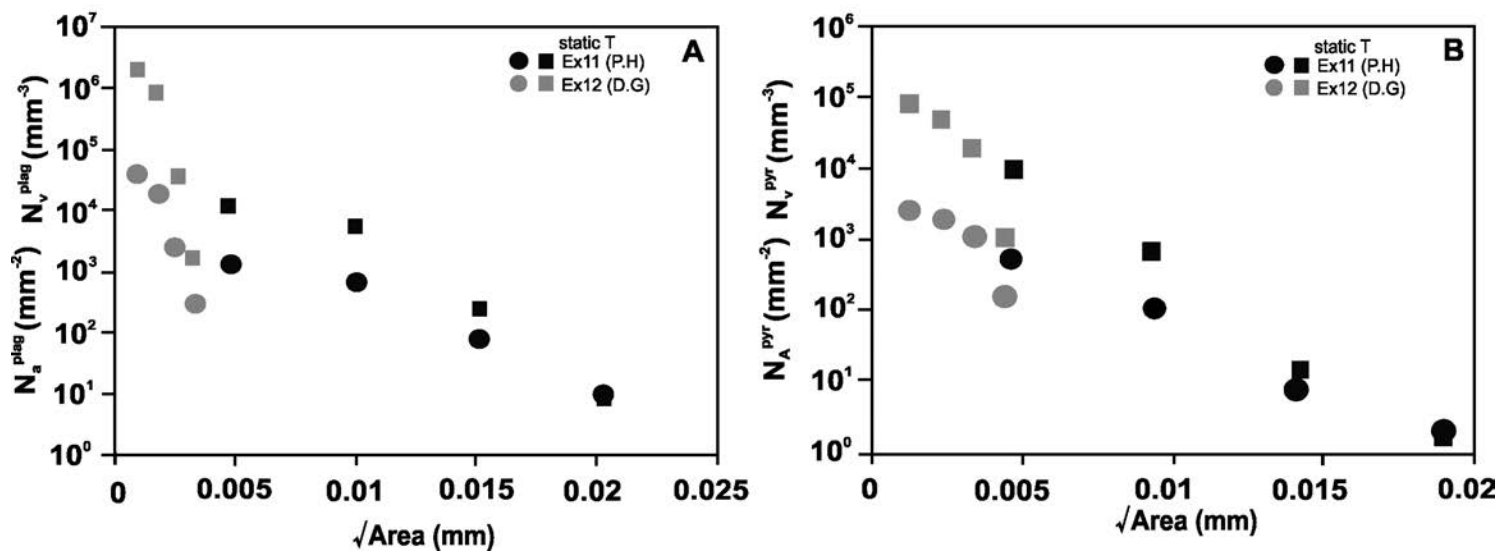
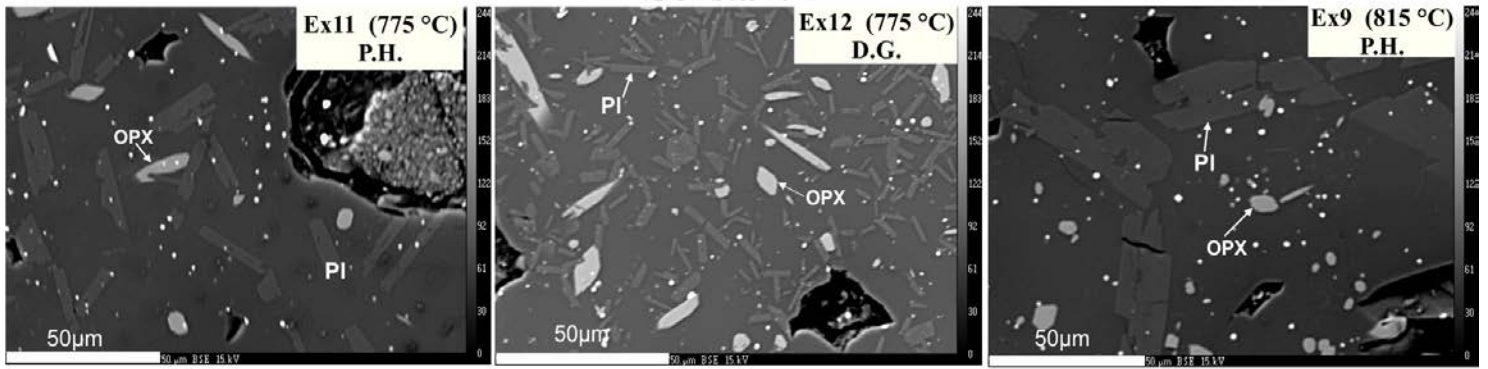


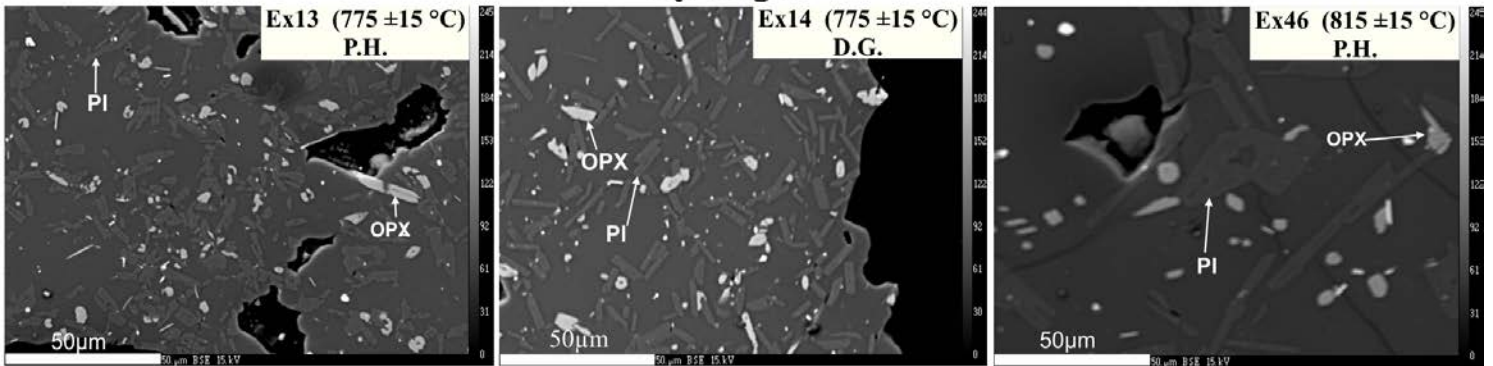


**Figure 4**

**Constant T**



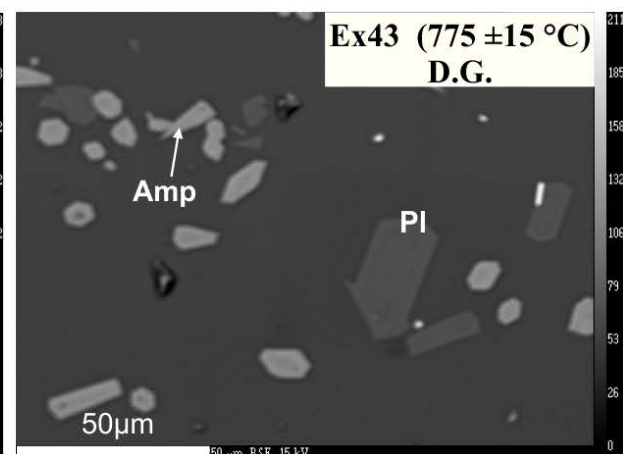
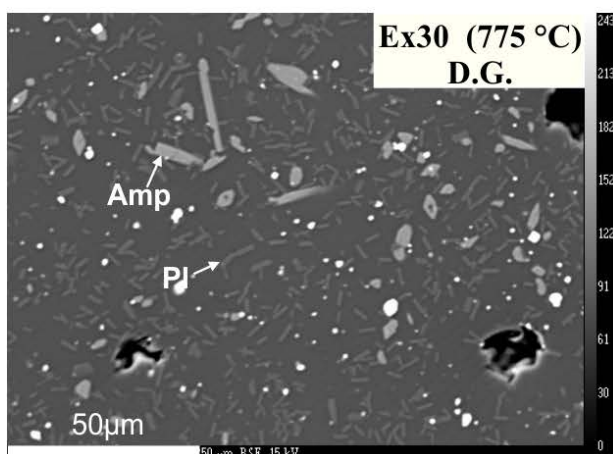
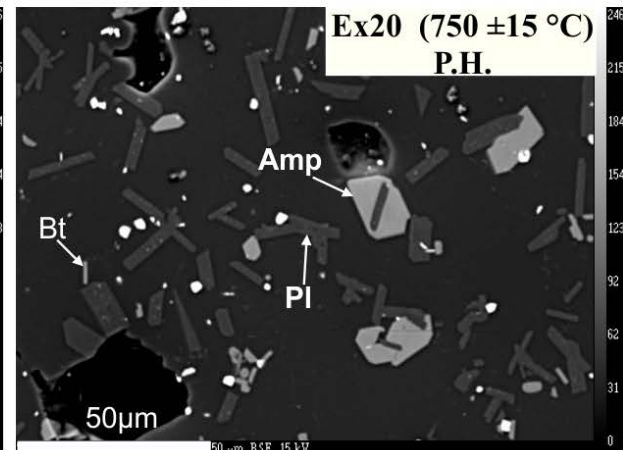
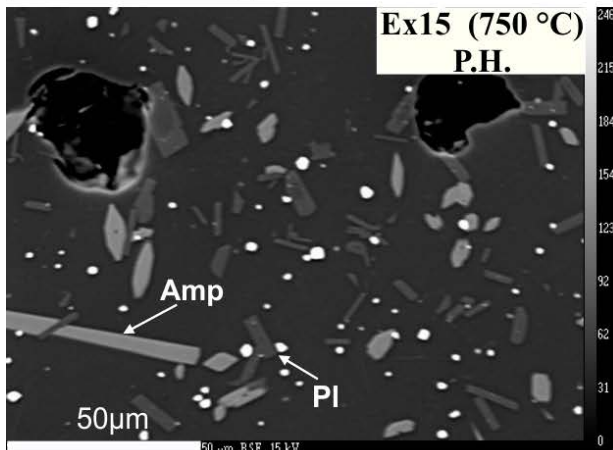
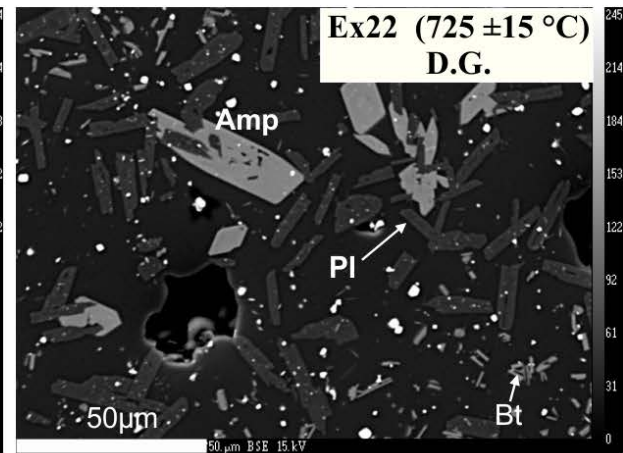
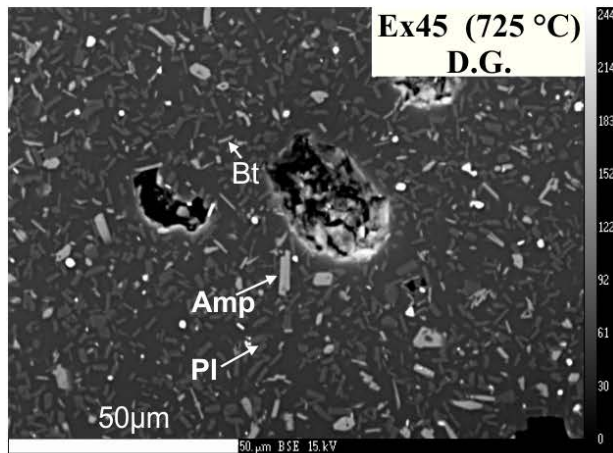
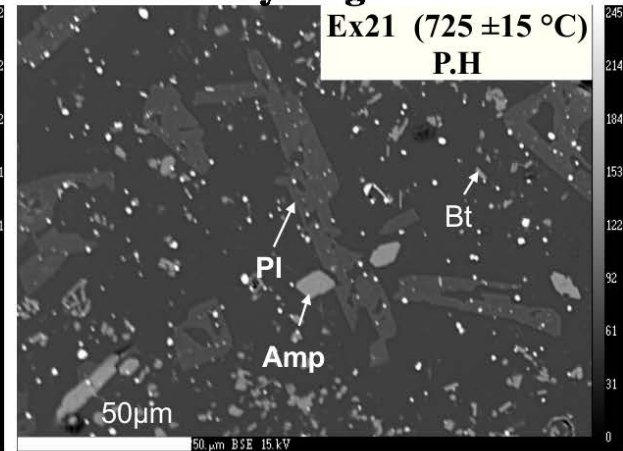
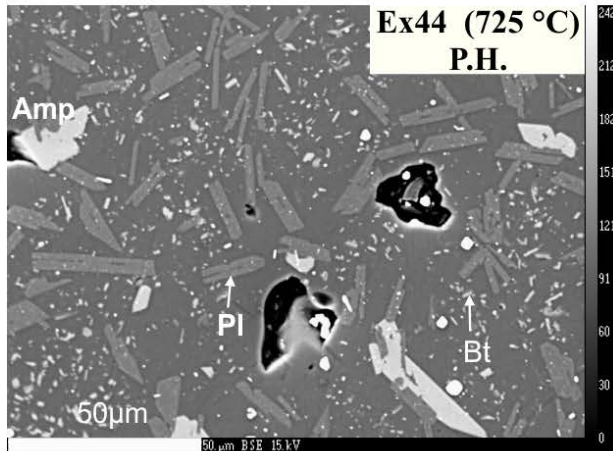
**Cycling T**



**Figure 5**

**Constant T**

**Cycling T**



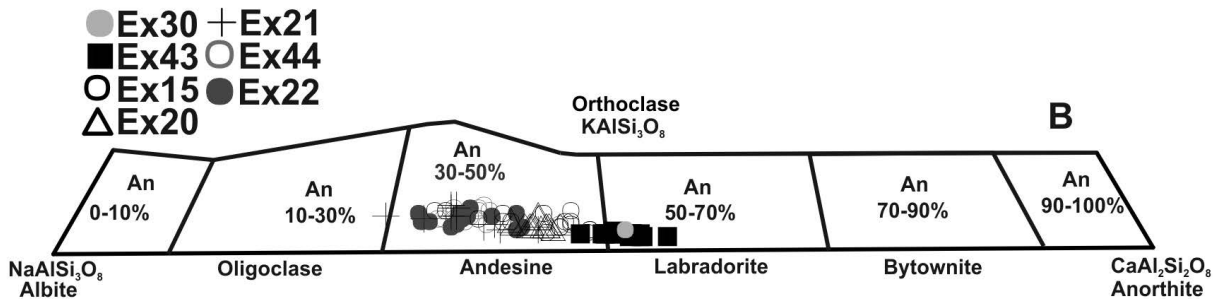
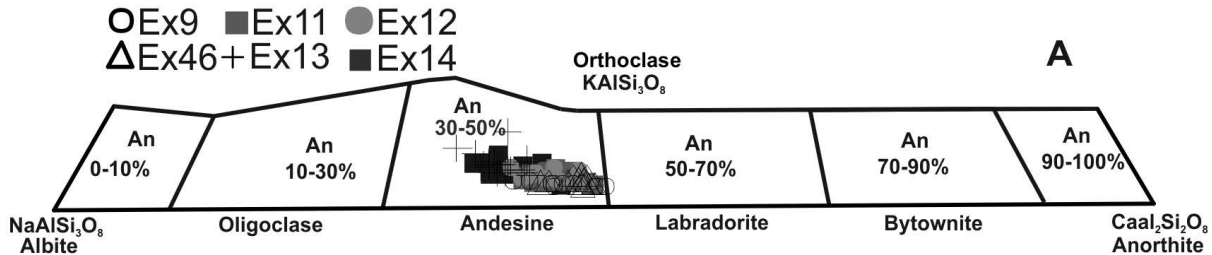


**Figure 7**

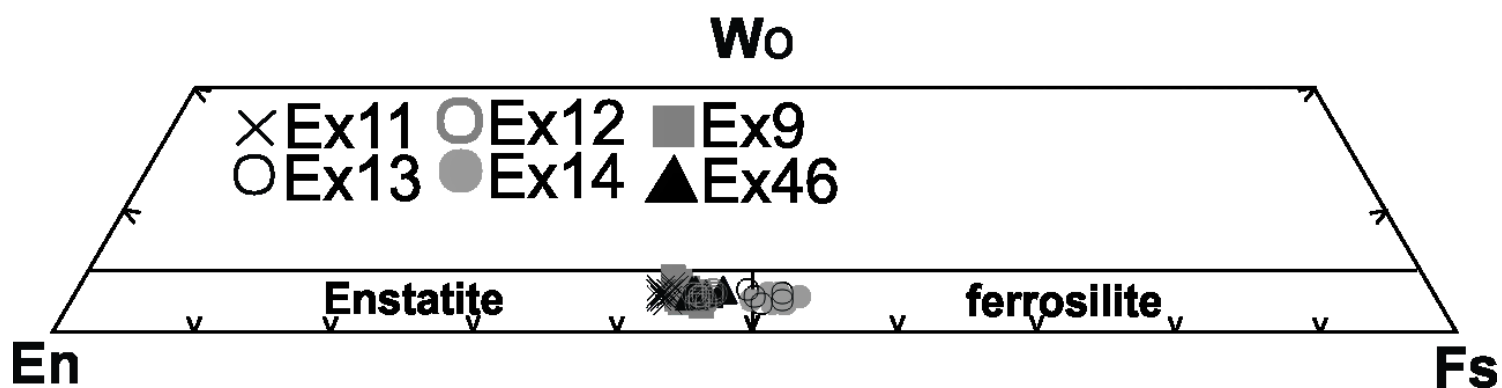


Figure 8

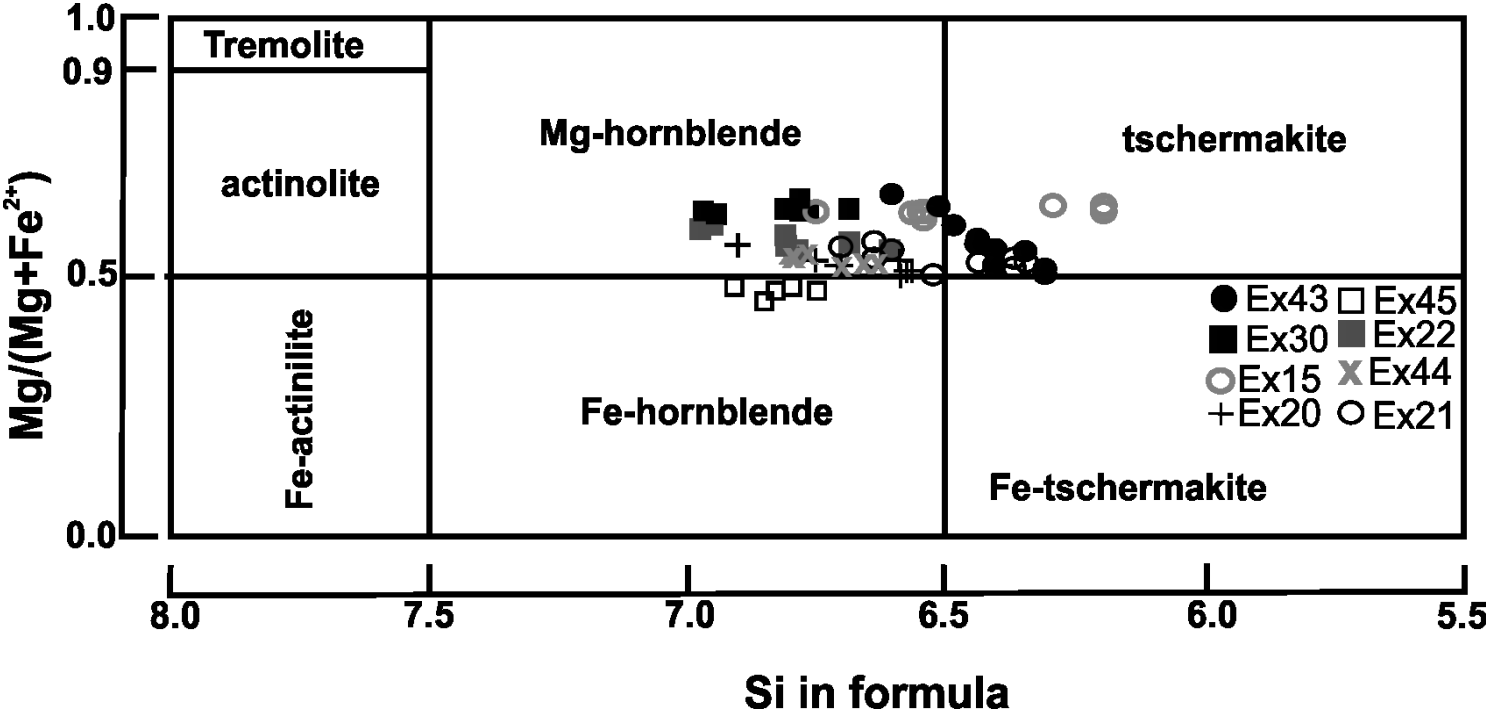


Figure 9

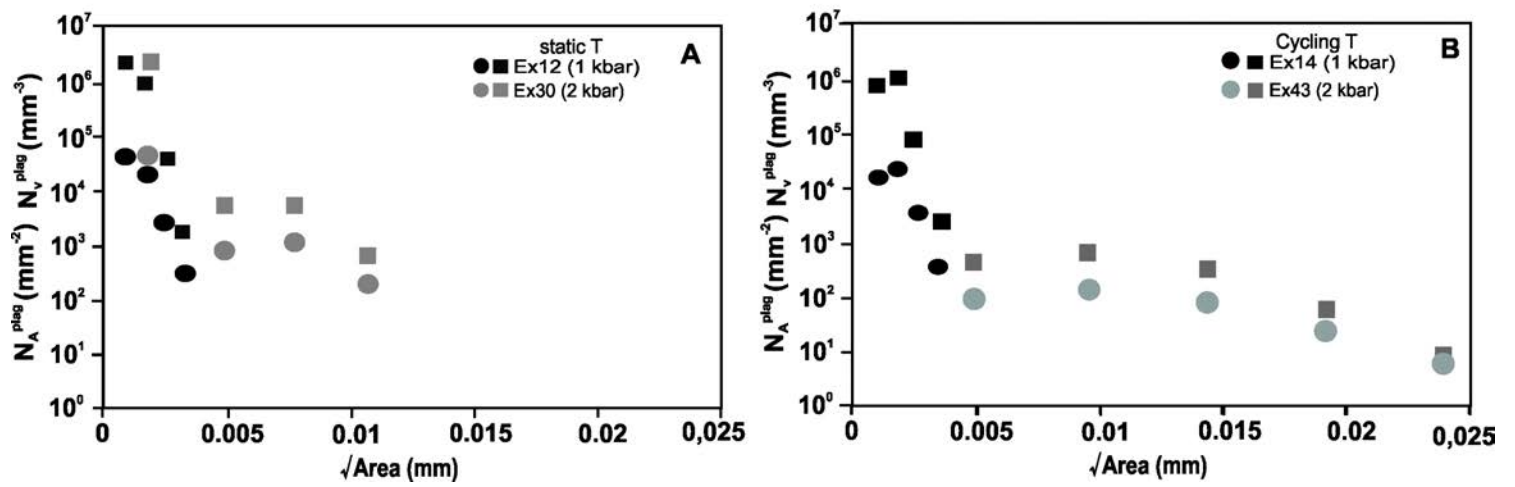


Figure 10

